 DOI: 10.1002/eji.201242730 Eur. J. Immunol. 2013. 43: 1208–1219

European Journal of Immunology

Tetraspanin CD37 contributes to the initiation of cellular immunity by promoting dendritic cell migration

Kate H. Gartlan[*1,2], *Janet L. Wee*[*1,3], *Maria C. Demaria*[1], *Roza Nastovska*[2], *Tsz Man Chang*[2], *Eleanor L. Jones*[1], *Vasso Apostolopoulos*[2], *Geoffrey A. Pietersz*[2,4], *Michael J. Hickey*[3], *Annemiek B. van Spriel*[5] *and Mark D. Wright*[1]

[1] Department of Immunology, Monash University, Prahran, Victoria, Australia
[2] Burnet Institute, Prahran, Victoria, Australia
[3] Department of Medicine, Centre for Inflammatory Diseases, Monash University, Victoria, Australia
[4] Department of Pathology, University of Melbourne, Parkville, Victoria, Australia
[5] Nijmegen Centre for Molecular Life Sciences, Radboud University Nijmegen Medical Centre, Nijmegen, The Netherlands

Previous studies on the role of the tetraspanin CD37 in cellular immunity appear contradictory. In vitro approaches indicate a negative regulatory role, whereas in vivo studies suggest that CD37 is necessary for optimal cellular responses. To resolve this discrepancy, we studied the adaptive cellular immune responses of CD37$^{-/-}$ mice to intradermal challenge with either tumors or model antigens and found that CD37 is essential for optimal cell-mediated immunity. We provide evidence that an increased susceptibility to tumors observed in CD37$^{-/-}$ mice coincides with a striking failure to induce antigen-specific IFN-γ-secreting T cells. We also show that CD37 ablation impairs several aspects of DC function including: in vivo migration from skin to draining lymph nodes; chemotactic migration; integrin-mediated adhesion under flow; the ability to spread and form actin protrusions and in vivo priming of adoptively transferred naïve T cells. In addition, multiphoton microscopy-based assessment of dermal DC migration demonstrated a reduced rate of migration and increased randomness of DC migration in CD37$^{-/-}$ mice. Together, these studies are consistent with a model in which the cellular defect that underlies poor cellular immune induction in CD37$^{-/-}$ mice is impaired DC migration.

Keywords: CD37 · Cellular immunity · Dendritic cells · Migration · Tetraspanins

Additional supporting information may be found in the online version of this article at the publisher's web-site

Introduction

Adaptive cellular immunity is initiated by presentation of foreign antigen by DCs to antigen-specific naïve T lymphocytes. DCs exist sparsely in peripheral tissues in a state specialized for antigen uptake and processing. However, upon pathogen encounter, DCs transduce signals through pattern recognition receptors, leading to an increased expression of cell surface molecules and cytokines, and induction of DC migration from the periphery to draining lymph nodes (DLNs) via afferent lymphatic vessels. Thus, upon their arrival in secondary lymphoid organs, DCs are equipped to initiate adaptive cellular immune responses through their ability to

Correspondence: Dr. Mark D. Wright
e-mail: Mark.Wright@monash.edu

*These authors contributed equally to this work.

activate naïve antigen-specific T cells [1]. Despite the importance of DC migration from the periphery to DLNs, the roles of the numerous molecules that regulate this process are incompletely understood.

One such molecule is the leukocyte-specific membrane protein CD37, a member of the tetraspanin protein superfamily. Tetraspanins molecularly organize cellular membranes by interactions with partner molecules, which they direct into regulated signal-transducing tetraspanin-enriched microdomains. The cellular processes regulated by tetraspanin-mediated molecular organization include proliferation, adhesion and migration [2, 3]. In immune cells, many important cell surface molecules, such as integrins, co-receptors, pattern recognition receptors and MHC molecules, are incorporated into tetraspanin-enriched microdomains [4–6].

CD37 has recently attracted interest as a target for monoclonal antibodies with therapeutic potential in B-cell malignancies [7, 8]. However, most of what is known about the contribution of CD37 to immunology has been gleaned from CD37$^{-/-}$ mice. The role of CD37 in immunity is complex, where it influences both innate and adaptive immunity. In innate immunity, CD37 molecularly interacts with pattern recognition receptor Dectin-1, stabilizing Dectin-1 at the macrophage cell surface, and negatively regulating proinflammatory cytokine secretion following ligand recognition [9]. Adaptive humoral immune responses are also perturbed by CD37 ablation. T-cell-dependent IgG responses are impaired in CD37$^{-/-}$ mice [10], due to the key role that CD37 has in transducing the α4β1 integrin-dependent akt signaling pathway in B cells [11]. Conversely, there is an exaggerated IgA response driven by an excess of IL-6 [12]. This exaggerated IgA production is significant as it protects CD37$^{-/-}$ mice from *Candida albicans* infection [12], but also leads to glomerulonephritis in ageing mice [13]. In cellular immunity, CD37 is one of multiple tetraspanins that negatively regulate T-cell proliferation, resulting in a hyperproliferative response of CD37$^{-/-}$ T cells stimulated in vitro [14]. In APCs, CD37 is one of a number of tetraspanins that molecularly associate with MHC class II (MHC-II) at the cell surface and has been shown to negatively regulate antigen presentation, as CD37$^{-/-}$ DCs are hyperstimulatory to antigen-specific T cells [15].

Given the impaired regulation of antigen presentation and T-cell proliferation in the absence of CD37 in vitro, one might predict an exaggeration of in vivo adaptive cellular immunity in CD37$^{-/-}$ mice. However, CD37$^{-/-}$ mice show no increased susceptibility to autoimmune induction and conversely, when combined with Tssc6 (Tspan32) deficiency, showed increased susceptibility to the mouse malarial parasite *Plasmodium yoelii* and poor antigen-specific T-cell responses to influenza infection [16]. It is clear from these findings that data derived in vitro are not predictive of the role of CD37 in immune responses in vivo.

In this study we examined the role of CD37 in in vivo adaptive cellular immune responses. CD37$^{-/-}$ mice were challenged with live and irradiated tumors, and soluble antigens coupled to the membrane-translocating peptide penetratin — all immunogens known to elicit powerful IFN-γ T-cell responses in WT mice. We show that CD37$^{-/-}$ mice make poor CD4$^+$ and CD8$^+$ T-cell IFN-γ responses to both tumor and model antigen challenge. Furthermore, we present evidence that CD37 ablation impairs various aspects of DC function including cell migration and adhesion. This study demonstrates that a defect in DC migration is a major cellular impairment that underlies poor cell-mediated and antitumor responses in CD37$^{-/-}$ mice.

Results

Impaired antitumor immunity and antigen-specific T-cell development in CD37$^{-/-}$ mice

Studies of pathogen resistance in CD37$^{-/-}$ mice suggested a role for CD37 during development of antigen-specific T-cell responses [16]. Since antigen-specific effector T cells are a critical requirement for tumor elimination [17], rejection of a syngeneic lymphoma-derived cell line transfected with the human cancer antigen Mucin 1 (RMA-Muc1) was compared between WT and CD37$^{-/-}$ mice. While RMA cells grow unchecked in mice of a C57BL/6 (WT) background (Fig. 1A), RMA-Muc1 cells provoke antigen-specific T-cell responses and tumor rejection typically within 2 weeks [18]. However, CD37$^{-/-}$ mice challenged with RMA-Muc1 failed to reject these tumors over a similar time course (Fig. 1B). Similarly, when challenged with fewer RMA-Muc1 cells, tumors grew significantly larger in CD37$^{-/-}$ mice than in their WT counterparts (Fig. 1C), indicating a role for CD37 in antitumor responses.

To compare development of antitumor T-cell responses in WT and CD37$^{-/-}$ mice, γ-irradiated RMA-Muc1 cells were injected i.d. and ELISPOT analyses performed 2 weeks later. While overall splenocyte numbers and leucocyte population frequencies did not differ between WT and CD37$^{-/-}$ mice (Supporting Information Fig. 1), the frequency of Muc1-specific IFN-γ-producing T cells induced in CD37$^{-/-}$ mice was significantly lower than that of WT mice (Fig. 2A), correlating with increased tumor growth observed in CD37$^{-/-}$ mice after RMA-Muc1 tumor challenge (Fig. 1). This defect was not T-cell subset restricted as shown by analyses of mice immunized with γ-irradiated B16 melanoma cells transfected to express ovalbumin (B16-OVA). The frequency of both CD4$^+$ and CD8$^+$ IFN-γ-secreting ovalbumin-specific T cells was significantly lower in CD37$^{-/-}$ mice compared with that of WT control mice (Fig. 2B).

To exclude any potential differences in antigen capture and processing in CD37$^{-/-}$ mice, similar experiments were performed with soluble antigens and peptides conjugated to the internalizing peptide penetratin [19]. Antp-OVA immunization induced a high frequency of IFN-γ-producing cells in WT mice, whereas this frequency was markedly lower in both CD4$^+$ and CD8$^+$ T-cell populations derived from CD37$^{-/-}$ mice (Fig. 2C). CD8$^+$ T-cell responses in CD37$^{-/-}$ mice were measured independently of T-cell help by immunization with Antp-SIINFEKL. Again, we observed a striking reduction in responding CD8$^+$ T-cell frequencies in CD37$^{-/-}$ mice suggesting that the defect in antigen-specific T-cell responses is not due to a failure of T-cell help (Fig. 2D).

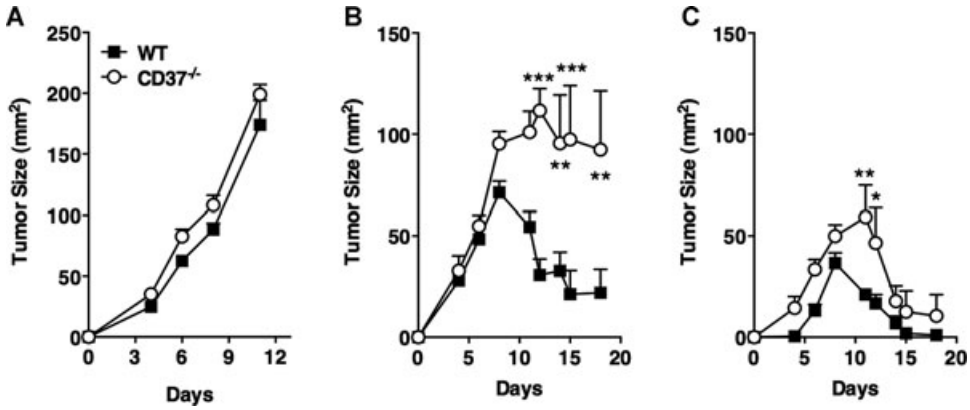

Figure 1. Increased tumor growth in CD37$^{-/-}$ mice. Tumor growth and rejection were compared in WT and CD37$^{-/-}$ mice by subcutaneous injection of either (A) 5×10^6 RMA, (B) 5×10^6 RMA-Muc1, or (C) 1×10^6 RMA-Muc1 lymphoma cells. Data are shown as mean ± SEM of $n = 5$ mice/group and are representative of four experiments performed. $^*p < 0.05$; $^{**}p < 0.01$, $^{***}p < 0.001$, two-way ANOVA with Bonferroni test.

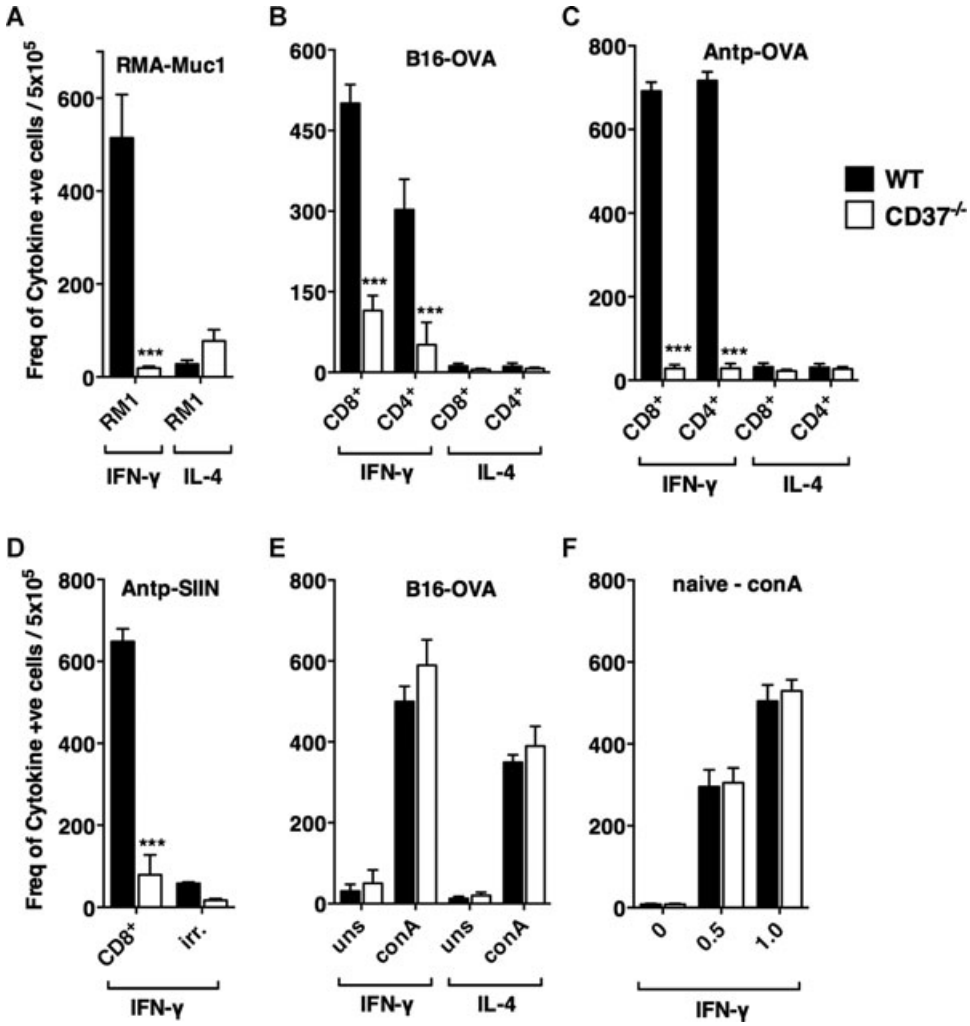

Figure 2. Antigen-specific T-cell responses are impaired in the absence of CD37. WT and CD37$^{-/-}$ T-cell responses were assessed by ELISPOT (A–E) after immunization or (F) in naïve mice. Immunized mice received either (A) γ-irradiated RMA-Muc1, (B, E) γ-irradiated B16-OVA, (C) soluble Antp-OVA, or (D) Antp- SIINFEKL peptide. Splenocytes were restimulated with either (A) γ-irradiated RMA-Muc1, (B–D) helper peptide (CD4$^+$), SIINFEKL peptide (CD8$^+$), or an irrelevant peptide sequence (Irr.), or (E–F) Con A. Antigen-specific IFN-γ or IL-4-secreting T-cell frequencies are shown and (E) Con A-stimulated splenocytes generated for each individual—B16-OVA immunized example shown. (F) Splenocytes from naïve mice were incubated in either media alone (unstim) or 0.5–1.0 μg Con A. Data are shown as the average frequency of cytokine-secreting cells + SEM of $n = 4$ mice/group (A–D) and $n = 6$–8 mice/group (E, F), and are representative of two to four experiments performed. $^{***}p < 0.001$, ANOVA with Bonferroni test.

Given Th1 (e.g., IFN-γ) and Th2 (e.g., IL-4) cytokine pathways are known to play cross-inhibitory roles [20], enhanced Th2 responses in CD37$^{-/-}$ mice may suppress IFN-γ production. However, IL-4 production was very low in both WT and CD37$^{-/-}$ mice (Fig. 2A–C). Similarly, an upregulation in antigen-specific IL-17-secreting T-cell frequencies (i.e., Th17) was not apparent (data not shown). Furthermore, these data could not be attributed to an intrinsic defect in cytokine production in CD37$^{-/-}$ T cells, as responses to con A, included as controls in all assays, were normal, regardless of whether splenocytes were harvested from immunized (Fig. 2E) or nonimmunized mice (Fig. 2F).

Impaired in vivo priming of antigen-specific T cells by CD37$^{-/-}$ DC

To explore the mechanisms underlying poor cellular immunity in CD37$^{-/-}$ mice, we first determined whether the CD37$^{-/-}$ immune system was able to elicit WT T-cell responses in vivo. Therefore, priming of adoptively transferred antigen-specific WT T cells (Ly5.1^{+}Vα2^{+}CD8α^{+}) in DLNs (Fig. 3A) was compared between WT and CD37$^{-/-}$ mice. While WT mice were able to efficiently drive proliferation of adoptively transferred OVA-specific OT-I T cells in vivo after immunization, induction of OT-I T-cell expansion and proliferation was significantly poorer in immunized CD37$^{-/-}$ mice (Fig. 3B–D). We conclude that CD37$^{+/+}$ T-cell priming is impaired in the absence of CD37, suggesting that a major defect in cellular immunity in CD37$^{-/-}$ mice resides in the cells with the unique ability to stimulate naïve T cells, namely DCs. To confirm this conclusion, bone marrow-derived dendritic cells (BMDCs) from WT and CD37$^{-/-}$ mice were pulsed with antigen and injected into WT and CD37$^{-/-}$ recipients to elicit immune responses measured by ELISPOT. The data confirm that CD37$^{-/-}$ BMDCs elicit significantly poorer IFN-γ T-cell responses than WT counterparts. Moreover, WT BMDCs are able to elicit strong responses in both WT and CD37$^{-/-}$ recipients, suggesting that CD37$^{-/-}$ T cells can respond efficiently to appropriate stimulation (Fig. 3E).

DC migration is impaired in the absence of CD37

Since we have previously established that CD37$^{-/-}$ DCs are potent inducers of T-cell responses in vitro [15] and that cytokine

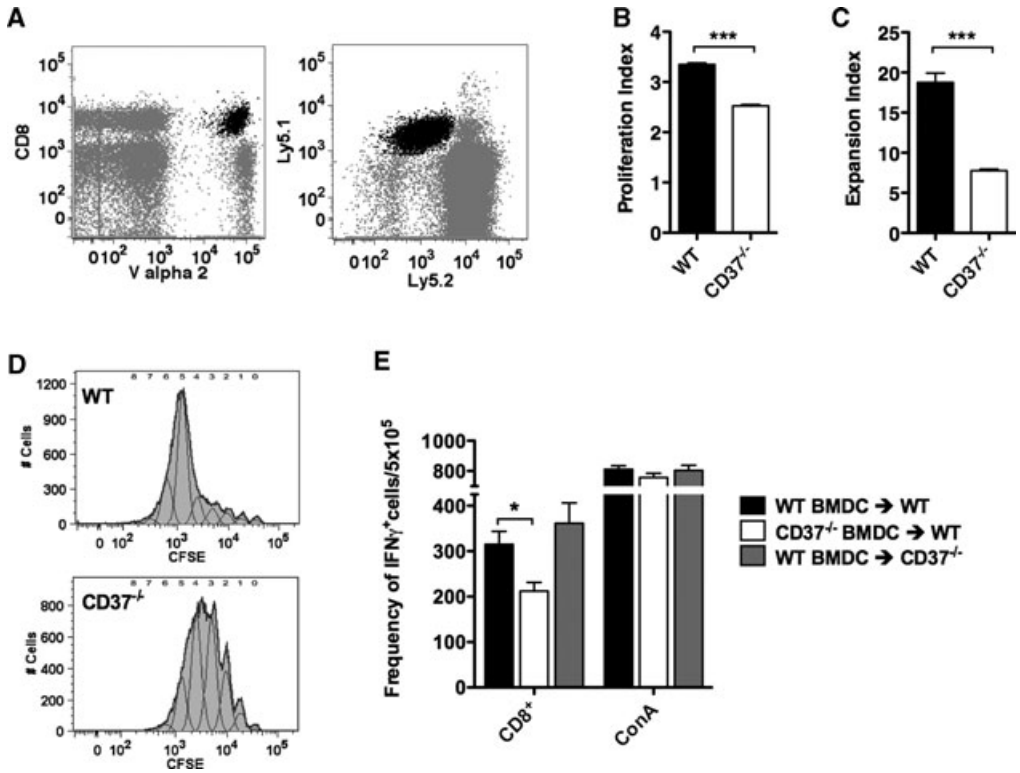

Figure 3. Impaired in vivo priming of WT T cells by CD37$^{-/-}$ DC. CFSE-labeled OT-I Ly5.1 cells were adoptively transferred into WT or CD37$^{-/-}$ mice 24 h prior to immunization with γ-irradiated B16-OVA cells. T-cell proliferative responses were assessed in the DLNs by flow cytometric analysis of CFSE dilution. (A) Antigen-specific OT-I T cells were gated on viable, CD8^{+}Vα2^{+}Ly5.1^{+} cells (black) and the (B) proliferation index and (C) expansion index of OT-I T cells after immunization of either WT or CD37$^{-/-}$ mice was determined. Histogram bars represent the mean + SEM of $n = 4$ mice/group; data are representative of four experiments. $^{***}p < 0.001$, two tailed t test. (D) Representative flow cytometry plots demonstrating cell division as detected by CFSE dilution (data = thick, gray-filled histogram, proliferation model = thin-line histogram). (E) SIINFEKL-pulsed WT or CD37$^{-/-}$ BMDCs were injected into WT or CD37$^{-/-}$ mice as indicated. Two weeks later splenocytes were harvested and restimulated with either SIINFEKL peptide (CD8^{+}) or Con A. The mean frequencies of antigen-specific IFN-γ-secreting T cells are shown as mean + SEM. WT BMDCs into WT recipients $n = 28$, CD37$^{-/-}$ BMDCs into WT recipients $n = 22$, WT BMDCs into CD37$^{-/-}$ recipients $n = 15$, data shown are pooled from six experiments performed. $^{*}p < 0.05$, ANOVA with Bonferroni test.

secretion (including the Th1 inducing IL-12p70) is unaltered in CD37$^{-/-}$ DCs (Supporting Information Fig. 2A), we assessed other DC functions known to be important in driving antigen-specific T-cell responses. Given that tetraspanins regulate cellular motility and adhesion in other cells [21, 22], a defect in DC migration may contribute to impaired antigen-specific T-cell development in CD37$^{-/-}$ mice. Therefore, the effects of CD37 deficiency were assessed in both in vivo and in vitro DC migration assays.

When DC migration from FITC-painted skin to the draining lymphoid tissue was monitored [23], FITC label was preferentially associated with migratory Langerhans and dermal DC populations (gates 1 and 2, respectively) in the DLNs (Fig. 4A), suggesting that these APCs had carried the FITC label from the periphery rather than FITC transfer to nonmigratory lymphoid resident populations (gates 3 and 4) [24]. When the absence of CD37 was assessed, a significant impairment of in vivo DC migration from the periphery to the LN was observed (Fig. 4B). Similarly, significantly fewer CD37$^{-/-}$ DCs emigrated from mouse ear explants in response to the chemokine CCL19 (Fig. 4C). This finding could not be attributed to a DC developmental defect, as the total number of CD11c^{+} CD37$^{-/-}$ DCs in ear tissue, enumerated by enzymatic digestion and release, was comparable with WT mice (Fig. 4D). To determine whether the defect in migration induced by CD37 ablation was intrinsic to DCs, or might be explained by defects in

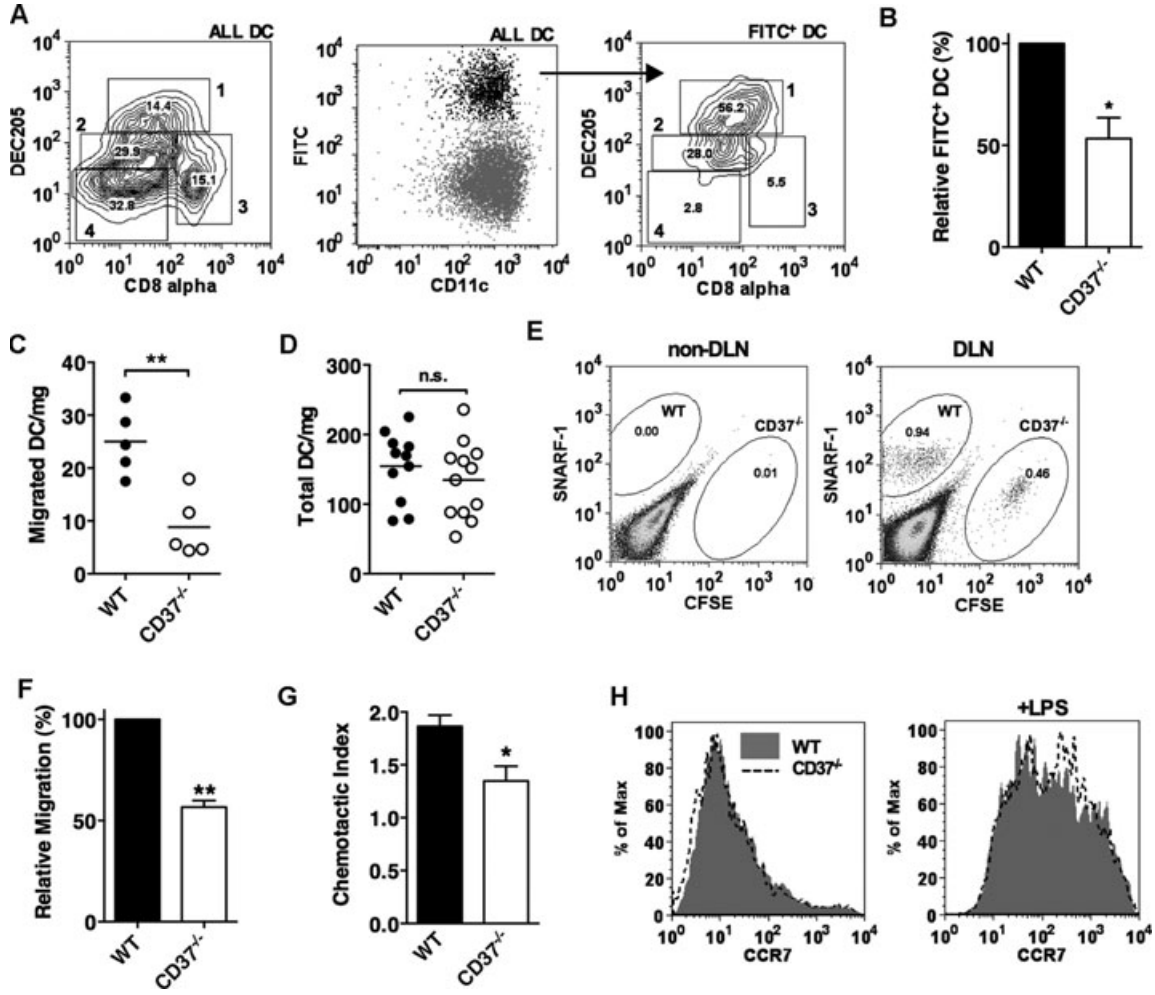

Figure 4. In vivo DC migration and in vitro chemotactic migration is impaired in the absence of CD37. (A–B) FITC staining was assessed in inguinal LN DCs 3 days after abdominal FITC skin painting. (A) Expression of DEC205 and CD8α by CD11c^{+} DLN DC subsets, demonstrating "skin derived" (gates 1–2) and "lymph node resident" DC (gates 3–4), was determined by flow cytometry. (B) Relative frequencies of FITC^{+}CD11c^{+} WT & CD37$^{-/-}$ DCs present in DLNs are shown as mean + SEM of $n = 7$ mice/group pooled from four experiments. (C) DC emigration from mouse ear tissue in response to CCL19 is shown. Each symbol represents an individual mouse and bars represent means; data are pooled from two experiments. (D) The total number of CD11c^{+} DCs/mg of ear tissue. Each symbol represents an individual mouse ear and bars represent means; data are pooled from three experiments. (E–F) Equal numbers of fluorescently-labeled WT (SNARF-1) and CD37$^{-/-}$ (CFSE) BMDCs were coinjected into recipient WT mice. (E) After 36–38 h, DCs were purified from draining and nondraining LNs and CD11c^{+} cells gated as shown. (F) Relative numbers of migrating CD37$^{-/-}$ DCs are expressed as a percentage of comigrating WT DCs and are shown as mean + SEM of $n = 4$ mice/group pooled from four experiments. (G) WT and CD37$^{-/-}$ BMDC migration was compared in vitro across Transwell inserts in response to 1 μM CCL19. The chemotactic index is shown as mean + SEM of five experiments. (H) Surface expression of CCR7 by WT and CD37$^{-/-}$ BMDCs was determined by flow cytometry in the presence and absence of LPS stimulation (1 μg/mL). Statistical analysis performed with (B, F) one-sample *t*-test, (C, D, G) two-tailed *t*-test, $^{*}p < 0.05$, $^{**}p < 0.01$.

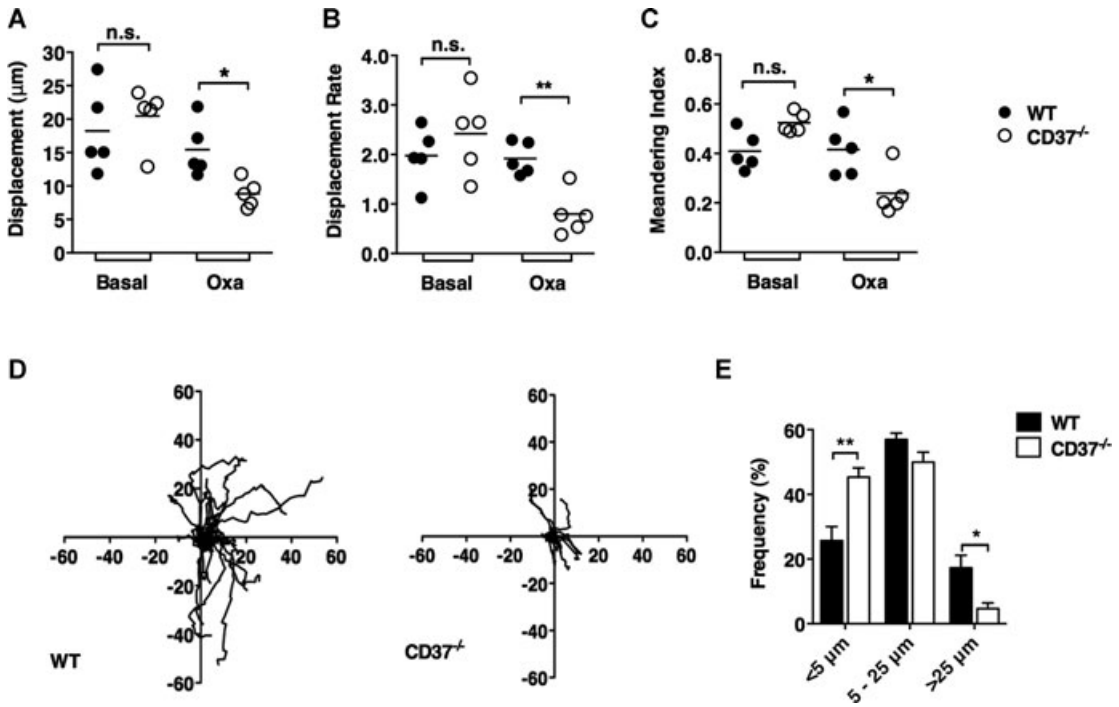

Figure 5. Two-photon confocal analysis of WT and CD37$^{-/-}$ dermal DC migration following treatment with oxazalone. (A–C) Comparisons of (A) displacement, (B) displacement rate, and (C) meandering index (displacement/track length), of WT and CD37$^{-/-}$ dermal DCs under basal conditions, or 18–20 h following application of oxazalone (Oxa) are shown. Data are derived from two separate areas within the abdominal flank, with ≥60 DCs per area evaluated from $n = 5$ mice/group. (D) Representative common origin plots of WT DCs (20 cells) and CD37$^{-/-}$ DCs (19 cells) traced over time by two-photon microscopy 18–20 h following oxazalone treatment. (E) The frequency of motile cells (based on displacement) at 18–20 h following oxazalone treatment is shown as mean + SEM of $n = 5$ mice/group, and is pooled from five experiments performed. *$p < 0.05$, **$p < 0.01$, two-tailed *t*-test.

CD37$^{-/-}$ microanatomy, WT, and CD37$^{-/-}$ BMDCs were differentially labeled, and coinjected intradermally into the same WT recipients. The frequency of injected CD37$^{-/-}$ DCs that migrated to DLNs was approximately half that of WT DCs (Fig. 4E and F). A DC intrinsic defect in migration was also observed for CD37$^{-/-}$ BMDCs during in vitro chemotaxis (Fig. 4G), where despite normal expression of CCR7 (Fig. 4H) and normal maturation responses to LPS (Supporting Information Fig. 2B), LPS-stimulated CD37$^{-/-}$ DCs displayed significantly poorer migration in response to CCL19.

Directional migration is impaired in CD37$^{-/-}$ DCs

To further examine the effect of CD37 deficiency on DC migration in vivo, CD37$^{-/-}$.CD11c-YFP mice were bred. CD11c-YFP mice express yellow fluorescent protein (YFP) selectively in DCs, enabling multiphoton microscopic visualization of dermal DCs in intact skin of live mice [25, 26]. Previous studies have demonstrated that dermal DC are spontaneously migratory [26]. Comparison of constitutive DC migration in WT and CD37$^{-/-}$ mice revealed no differences in basal migration parameters including distance, velocity, and straightness of migration (as indicated by displacement, displacement rate, and meandering index, Fig. 5A–C). Since the in vivo findings suggest a deficiency in migration of CD37$^{-/-}$ DCs when performed under activatory conditions, such as dibutyl phthalate application or immunization, we next characterized the DC response to the chemical irritant oxazolone. Comparison of WT and CD37$^{-/-}$ DC migration 18–20 h after oxazolone treatment revealed significant reductions in migratory function and random migration in CD37$^{-/-}$ DCs (see Oxa, Fig. 5A–C). This is further illustrated by comparison of the *XY*-displacement tracks of DC migration in WT and CD37$^{-/-}$ mice, which show extensive paths of migration in WT mice, in contrast to minimal responses in CD37$^{-/-}$ mice (Fig. 5D). In addition, a significant proportion of CD37$^{-/-}$ DCs were less motile displaying an increased frequency of cells with <5 μm displacement (Fig. 5E). Videos showing this impaired in vivo directional migration of CD37$^{-/-}$ DCs compared with that of WT controls are included in the Supporting Information (Supporting Information Fig. 3 and 4). Taken together, Figure 4 and 5 demonstrate that CD37 ablation induces a significant impairment in DC migration.

Adhesion and cell spreading is impaired in CD37$^{-/-}$ DCs

Tetraspanins molecularly associate with integrins and regulate outside-in signaling and cytoskeletal rearrangement as evidenced by impaired adhesion strengthening under flow and cell spreading observed in tetraspanin-deficient cells [27–31]. To test if CD37 plays a similar role in DCs, we first measured DC adhesion to ECM substrates under low shear flow conditions. WT DCs adhered

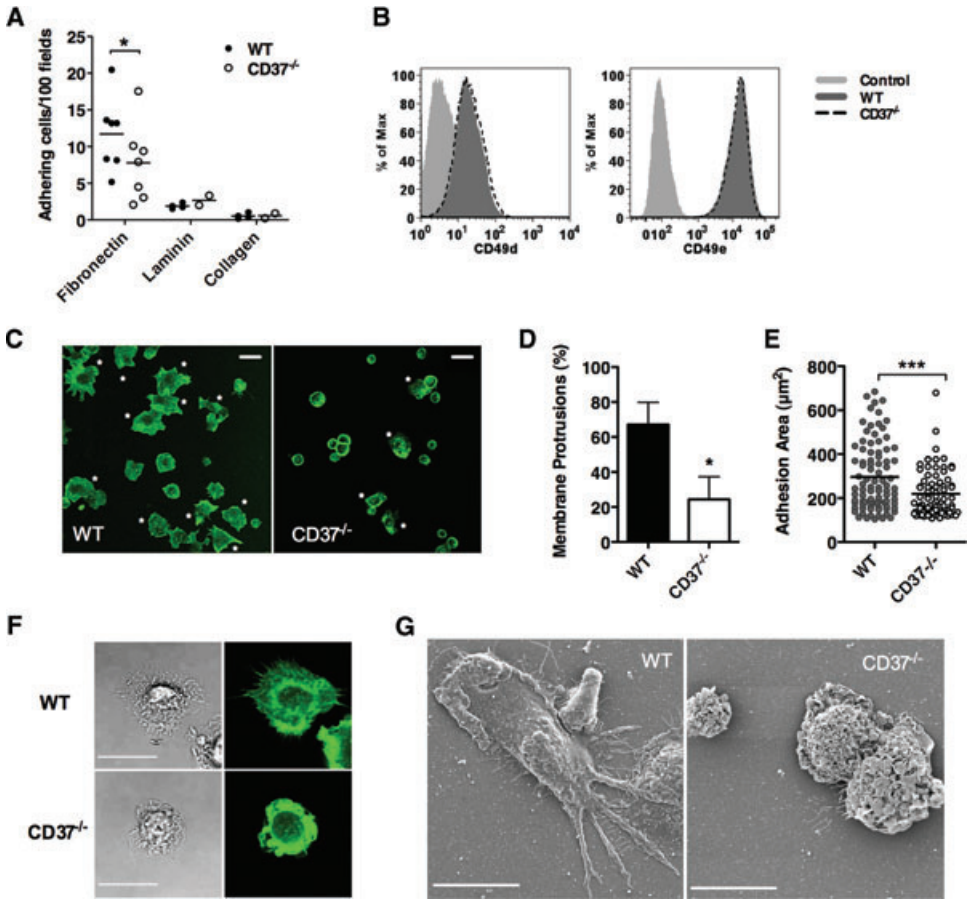

Figure 6. BMDC adhesion and cell spreading is impaired in the absence of CD37. (A) WT and CD37$^{-/-}$ BMDCs were perfused over fibronectin, collagen, or laminin-coated flow chambers and adherent cells/100 fields recorded over the length of the flow chamber. Each symbol represents a single experiment and the bar represents the mean. $^{*}p < 0.05$, two-tailed *t*-test (Fibronectin: $n = 7$ experiments, Laminin & Collagen: $n = 4$ experiments WT and $n = 2$ experiments CD37$^{-/-}$). (B) Flow cytometric analysis of cell surface integrin expression by WT (dark gray-filled histogram) and CD37$^{-/-}$ (black dashed-line histogram) BMDCs. (C)–(E) LPS-stimulated BMDC membrane morphology was characterized following adhesion to fibronectin in the presence of PMA. (C) Representative fluorescence micrographs of BMDCs postfibronectin adhesion stained with Phalloidin-FITC (scale bars = 20 μm). White asterisks indicate example cells displaying cell spreading/membrane protrusions. (D) The frequency of BMDCs with membrane protrusions was determined from a total of 180–200 cells in each experiment and is shown as mean + SEM of data pooled from $n = 3$ experiments. $^{*}p < 0.05$, two-tailed *t*-test. (E) Cell adhesion areas were calculated from Phalloidin- FITC labeled fluorescence micrographs as in (C). Symbols represent individual cells, bars represent mean, and data are representative of three experiments $n = 100$ cells/group, $^{***}p < 0.001$, two-tailed *t*-test. (F) LPS-stimulated WT and CD37$^{-/-}$ BMDCs were adhered to fibronectin coated coverslips, stained with Phalloidin-FITC and visualized by bright-field (left) and confocal (right) microscopy (scale bar = 20 μm). (G) LPS-stimulated WT and CD37$^{-/-}$ BMDCs were adhered to fibronectin-coated coverslips and visualized by scanning electron microscopy (scale bar = 20 μm). (C, D, F, G) Data shown are representative of 8–15 fields examined, 2 experiments performed.

efficiently to fibronectin, but poorly to laminin and collagen (Fig. 6A). However, despite normal expression of the fibronectin receptors CD49d and CD49e integrins (Fig. 6B), the absence of CD37 resulted in significantly reduced BMDC fibronectin adhesion (Fig. 6A). Cell spreading upon adhesion and membrane protrusion formation are dependent on cytoskeletal rearrangement driven by actin polymerization. To assess the role of CD37 in these processes, activated BMDCs were allowed to adhere and spread on fibronectin. Actin-dependent cell spreading was visualized by Phalloidin staining (Fig. 6C and F), bright field imaging (Fig. 6F), and scanning electron microscopy (SEM) (Fig. 6G). The percentage of cells with membrane protrusions and the area of adhered cells were quantitatively determined (Fig. 6D and E). While WT DC readily spread, formed membrane protrusions and showed a classical dendritic morphology, CD37$^{-/-}$ DCs had a smaller rounded morphology with a relative absence of protrusive membranes (Fig. 6C–G). We conclude that CD37 is essential for cytoskeletal-dependent processes such as adhesion under flow, cell spreading upon adhesion, and the formation of membrane protrusions.

Discussion

CD37$^{-/-}$ mice display poor adaptive cellular responses to live tumors, irradiated tumors, and soluble antigens (Fig. 1 and 2). These findings are difficult to reconcile with exaggerated T-cell proliferative [14] and DC antigen-presenting phenotypes [15]

observed when examining CD37-deficient cells in vitro. Classically, effective adaptive cellular immunity to tumors is characterized by the induction of $CD8^+$ cytotoxic T lymphocytes, helped by IFN-γ-secreting Th1 $CD4^+$ T cells. CD37 negatively regulates T-cell proliferation [14]; therefore, a contribution of aberrant T lymphocytes to poor $CD37^{-/-}$ cellular responses observed in $CD37^{-/-}$ mice must be considered. However, it is difficult to argue that in vitro hyperproliferation could manifest in vivo as an inability to mount an effective IFN-γ response. The defect is not due to an inherent inability of stimulated $CD37^{-/-}$ T cells to secrete IFN-γ (Fig. 2E–F and 3E), to altered frequencies of T cells such as Treg cells (Supporting Information Fig. 1), or to skewing of $CD37^{-/-}$ T-cell responses away from an IFN-γ-secreting Th1 cell phenotype. IL-12 is produced normally in $CD37^{-/-}$ DCs (Supporting Information Fig. 2) and T-cell IL-4 (Fig. 2A–C) responses were minimal for both WT and $CD37^{-/-}$ mice. Moreover we could detect no defects in activated $CD37^{-/-}$ T-cell homing to lymphoid organs (data not shown).

By contrast there are several lines of evidence that point to an impairment in DC migration in $CD37^{-/-}$ mice. First, despite $CD37^{-/-}$ DCs being potent stimulators of T cells in vitro [15], immunized $CD37^{-/-}$ mice show impaired priming of adoptively transferred WT T cells, and $CD37^{-/-}$ DC induce poor T-cell responses when injected into WT recipients, showing a defect in the biology of $CD37^{-/-}$ DC in vivo (Fig. 3). Second, in vivo and in vitro experiments point to a significant impairment in migration that was intrinsic to $CD37^{-/-}$ DCs (Fig. 4). This observation was extended by in vivo visualization of DC migration in WT and $CD37^{-/-}$ mice, via multiphoton confocal microscopy (Fig. 5). Initial experiments revealed no difference in spontaneous dermal DC migration, consistent with the absence of a phenotypic difference between WT and $CD37^{-/-}$ naïve mice [10]. Subsequently, we examined the response of dermal DCs to a local inflammatory irritant, oxazolone. The WT response to this treatment was a period of cessation of DC migration, as described previously for DCs that encounter danger signals [26], followed by a recovery of migration some hours later. As DCs typically migrate to the LN following local inflammatory stimulation, the latter response presumably models this phase of DC behavior. The absence of CD37 had its most significant effect on DC migration during this second phase, reducing both the velocity and directionality of migration. The combination of these two deficits would be expected to markedly reduce the efficiency of DC migration toward dermal lymphatics en route to the LN, a hypothesis supported by analysis of both in vivo DC migration in the FITC painting model (Fig. 4A), and the poor recovery of injected $CD37^{-/-}$ BMDCs in DLNs (Fig. 4E–F). Taken together, the evidence supports a model where an impairment in DC migration is a major contributing factor to the poor adaptive cellular immunity induced in $CD37^{-/-}$ mice; the $CD37^{-/-}$ DCs do not arrive in DLNs in sufficient numbers to effectively induce an adequate cellular immune response.

The study of molecules that regulate DC migration is an area of intense investigation and DC migration occurs via both adhesion-dependent [32–34] and adhesion-independent mechanisms [35], the latter driven by a chemokine-dependent mechanism involving cytoskeletal rearrangement [36]. Tetraspanins can potentially contribute to both adhesion-dependent and adhesion-independent DC migration. Tetraspanins are best characterized by their ability to molecularly interact with integrins — adhesion molecules important in regulating cell migration in many diverse cell types [2]. Tetraspanins regulate integrin function, as frequently observed in the impaired adhesion and migration of tetraspanin-deficient cells of various lineages [27, 29–31]. Similarly, we demonstrate that adhesion to fibronectin is impaired in $CD37^{-/-}$ DCs under low shear flow (Fig. 6A) implicating a role for CD37 in regulating outside-in signaling of α4β1 and/or α5β1 integrins in DCs.

Tetraspanins are also known to interact with the cytoskeleton via molecular interactions with ezrin/radixin/moesin proteins [37], and cross-linking tetraspanins at the cell surface can drive cytoskeletal rearrangement [38]. In this study we observed impaired $CD37^{-/-}$ DC function in two processes known to require cytoskeletal rearrangement: integrin outside-in signaling, investigated by measuring adhesion under flow (Fig. 6A), as well as cell spreading to form membrane protrusions (Fig. 6C–G). An effect of CD37 ablation on cytoskeletal rearrangement is also consistent with a recent report that the absence of another tetraspanin, CD81, results in inhibited integrin-dependent in vitro DC chemotaxis [28] and the formation of membrane protrusions, driven by a dysregulation of Rac-1 activation. While the in vivo immunological effects of impaired migration of $CD81^{-/-}$ DCs were not studied [28], in the present paper it is clear that CD37 ablation profoundly affects in vivo DC migration which is the likely cellular mechanism that underlies the poor cellular immunity induced in $CD37^{-/-}$ mice. The next challenge is to unravel the molecular interactions of CD37 in DCs.

Materials and methods

Mice

C57BL/6 (WT), C57BL/6.$CD37^{-/-}$ ($CD37^{-/-}$) [10], CD11cYFP, $CD37^{-/-}$.CD11cYFP, and OT-I Ly5.1 mice were bred in house, or obtained from the Walter and Eliza Hall Institute (Melbourne, Australia). Mice were housed under SPF conditions within the Burnet Institute animal facility (Austin Campus), the AMREP Animal Services, or the Nijmegen Medical Centre and used between 8 and 12 weeks of age. In vivo multiphoton imaging was performed on 8–10-week-old female $CD37^{-/-}$.CD11cYFP mice with CD11cYFP mice used as controls. The corresponding campus animal ethics committees at Austin Hospital, AMREP Animal Services, Monash Medical Centre, or Nijmegen Medical Centre approved all animal experiments.

Tumor challenge

Mice were challenged subcutaneously with 1–5 × 10^6 cells from either RMA (C57BL/6 — T-cell lymphoma) or RMA-Muc1 as

described previously [39]. Mucin-1 expression in RMA-Muc1 cells was maintained during culture by hygromycin treatment and assessed via flow cytometry. Tumor growth was measured by calipers daily. Mice with tumors in excess of 2.0 cm^2 were culled from experiments for ethical reasons.

Immunizations and antigen preparation

Mice were immunized with the following antigens via base of tail intradermal injection: (i) model tumors: 5×10^6 γ-irradiated RMA-Muc1 cells or ovalbumin expressing B16 tumor cells (B16-OVA), (ii) Antennapedia peptide conjugated antigens: 25 μg Antp-OVA or Antp-SIINFEKL [39] or (iii) 1–2 $\times$ 10^6 WT or $CD37^{-/-}$ LPS-activated BMDCs pulsed with 1 μg/mL SIINFEKL (Mimotopes) for 1 h at 37°C.

Antigen-specific cytokine responses (ELISPOT)

Two weeks after immunization, 5×10^5 splenocytes were stimulated in triplicate with either 2.5 μg/mL con A, 20 μg SIINFEKL peptide, 20 μg Helper peptide, or 2×10^5 irradiated RMA-Muc1 cells [39]. Naïve splenocytes were stimulated in triplicate with 0.5–1.0 μg/mL Con A. Negative controls were included in all assays as irrelevant peptides, unstimulated splenocytes, and nontransfected RMA cells. IFN-γ-secreting T cells were detected with mAbs RA-642 and XMG1.2 (BD Pharmingen) and the mAbs 11B11 and BVD6–24G2 (BD Pharmingen) were used to detect IL-4 production. The AID ELISPOT Reader System (Autoimmun Diagnostika) was used to quantify the frequency of cytokine producing T cells.

DC isolation and in vitro derivation

Splenic DCs were isolated by enzymatic digestion and density-gradient centrifugation followed by magnetic bead depletion [15]. BMDCs were generated from 7 to 9 day cultures supplemented with 10 ng/mL GM-CSF and IL-4 (R&D Systems) and stimulated with 1 μg/mL LPS for 17–20 h. Purity was determined by mAbs detecting CD11c and MHC-II expression resulting in >85% $CD11c^+MHC\text{-}II^+$.

In vivo T-cell proliferation

T cells were purified from OT-I Ly5.1 mice via mAb cocktail [14] and bead depletion (Qiagen) and labeled with CFSE before adoptive transfer (i.v.) of 3×10^6 cells into WT or $CD37^{-/-}$ mice. After 24 h, recipient mice were immunized intradermally with γ-irradiated B16-OVA cells. Five days later, mice were culled and inguinal LNs stained with CD8α, Vα2, Ly5.1, and Ly5.2 mAbs before flow cytometric analysis.

In vivo DC migration

Fluorescein-5-isothiocyanate (FITC "Isomer I") (Invitrogen) was dissolved in DMSO at 10% w/v. Acetone and dibutyl phthalate were added at a 1:1 ratio to make up a final 1% w/v FITC solution. FITC (100 μL) was applied to the shaved abdominal region of mice and after 3 days DCs purified from inguinal (draining) and brachial (nondraining) LN via positive selection with anti-CD11c labeled magnetic beads (Miltenyi Biotec). Cells were stained for CD11c, CD8α, and DEC205 expression and gated on $CD11c^+$ cells. The frequency of $FITC^+$ DCs detected in the DLN was normalized to WT migration.

BMDC homing to DLNs was compared between fluorescently labeled WT and $CD37^{-/-}$ cells (0.5 μM CFSE or 1 μM SNARF-1, Molecular Probes). A total of 1×10^6 labeled WT and $CD37^{-/-}$ BMDCs were coinjected intradermally (base of tail) into WT mice. Approximately 36 to 38 h later, DLNs (inguinal) and non-DLNs (brachial) were harvested, digested with DNase (1 mg/mL) and collagenase (1 mg/mL), centrifuged over Nycodenz gradients, and the enriched DC preparations stained for CD11c expression. The relative frequencies of $CD11c^+CFSE^+$ and $CD11c^+SNARF\text{-}1^+$ cells were assessed by flow cytometry and results confirmed in reciprocal labeling experiments.

Ex vivo DC migration

Mouse ears were excised and weighed prior to being split into dorsal and ventral halves. Right ears were placed in culture medium containing CCL19 (1 μM) and left ears in medium alone and cultured for 24 h at 37°C. Emigrated cells were harvested, stained for CD11c expression, and enumerated via FACS in the presence of counting beads (BD Biosciences). Ex vivo DC chemotaxis was calculated as the number of $CD11c^+$ cells/mg of excised ear tissue emigrating in response to CCL19 corrected for DC emigration in response to medium alone. The total number of DC per ear was determined in separate assays in which ear tissue was homogenized and digested with DNase (1 mg/mL) and collagenase (0.1 mg/mL) for 60–90 min at 37°C. The resulting single cell suspensions were stained for CD11c expression and DCs enumerated with counting beads via FACS.

In vitro DC migration and adhesion

In vitro DC migration was examined using trans-well assays. LPS (1 μg/mL) stimulated BMDCs were incubated in the upper chamber of trans-wells (5 μm pore size; Costar) at 5×10^5 cells per well, with medium alone or medium containing CCL19 (1 μM) in the lower chamber. After 2 h incubation, cells in the upper chamber were discarded and migrated DCs in the lower chamber harvested. $MHC\text{-}II^+CD11c^+$ DCs were enumerated with counting beads via FACS. The results are presented as chemotactic index whereby the number of cells migrating to CCL19 is normalized to number of cells migrating randomly (no CCL19).

BMDC adhesion was examined using parallel flow chamber assays. BMDCs (1.5×10^6 cells/mL) diluted in HBSS containing Ca^{++} and Mg^{++} were perfused at a low physiological shear rate of 0.5 dynes/cm^2 through a flow chamber (at 37°C) precoated with extracellular matrix proteins (10 μg/mL), then blocked with 1% BSA-PBS prior to use. Following a 2 min perfusion to initiate cell adhesion, the number of adherent cells per (10×) microscopic field was determined by image analysis of video-recordings made along the length of the flow chamber over 5–6 min. Results were expressed as the number of BMDCs adhering per 100 fields examined.

BMDC adhesion morphology was assessed by bright-field, fluorescence, confocal, and SEM, in which BMDCs were incubated in the presence of 50 ng/mL PMA (Sigma-Aldrich) on human fibronectin coated coverslips (Sigma-Aldrich; 50 μg/mL in PBS), for 1 h at 37°C. Cells were fixed prior to imaging with 4% paraformaldehyde (bright-field, fluorescence & confocal) or 2.5% glutaraldehyde-100 mM cacodylate buffer (SEM). Filamentous actin (F-actin) was detected by Phalloidin-FITC (Sigma-Aldrich; 0.5 μg/mL) following fixation and 0.1% Triton-X permeablization. A total of 180–200 F-actin-labeled DCs were visualized (at 400× magnification) and blind scored to determine the frequency of cells displaying membrane protrusions. The extent of cell spreading following 1-h incubation on fibronectin was assessed by determining the surface area of Phallodin stained cells imaged by fluorescent microscopy. Cell–cell contact and debris artifacts were removed using ImageJ software (NIH). SEM samples were dehydrated through a series of ethanols and critically point-dried. After sputter coating with gold, the cells were examined using a JOEL JSM 6390 scanning electron microscope.

In vivo multiphoton imaging

Mice were either left untreated or given a single application of 50 μL of 5% oxazolone (4-ethoxymethylene-2-phenyl-2-oxazolin-5-one; Sigma-Aldrich) in an acetone/olive oil vehicle (4:1) to a 20 × 10 mm area of shaved skin on the left abdominal flank. 18 h later, abdominal flank skin was prepared [40, 41] and multiphoton imaging performed. Briefly, mice were anesthetized (ketamine hydrochloride, 150 mg/kg; xylazine hydrochloride, 10 mg/kg) and a heat pad used to maintain body temperature. A jugular vein was cannulated for anesthetic administration. A midline skin incision was made and the flank skin and associated vasculature separated from underlying connective tissue and extended over a heated pedestal using sutures attached to the margin. The exposed area of the hypodermis was immersed in saline and sealed with a coverslip held in place with vacuum grease. Preparations were viewed on a Leica SP5 confocal microscope (Leica Microsystems, Mannheim, Germany) equipped with a 20× 1.0 NA water immersion objective lens, four nondescanned detectors, and a SpectraPhysics MaiTai laser. Preparations were excited at 900 nm, and two separate regions within the abdominal flank were imaged to a depth of ~100 μm for 30 min. DCs were identified as YFP-positive cells and DC migration parameters such as displacement, track length, migration velocity, and meandering index (displacement/track length), were derived via IMARIS software (Bitplane Scientific Software). Common origin graphs were generated by plotting *XY* positions (starting points normalized to $X = 0$, $Y = 0$) taken from all cells present in a single field measured for 35 consecutive positions.

Statistics

Statistical comparisons of in vivo experiments were performed by either two-tailed student *t*-tests or, when multiple comparisons were made, ANOVA with appropriate posttests as described. When in vitro comparisons were made, experiments were performed multiple times as described and technical replicates/mice averaged prior to comparisons between strains. The *n* value used to generate SEM error bars is reported in the corresponding figure legend and refers to either the number of mice per group, or the number of experiments as described. Statistical analyses were performed with Prism 5 software (GraphPad).

Acknowledgments: This work was funded by grants from the Australian National Health & Medical Research Council (Project grant #546017 and #1033198), the Anti Cancer Council of Victoria and the Association of International Cancer Research (06–262), the Dutch Cancer Society (KWF Grant 2007–3917 to A.V.S), and the Netherlands Organization for Scientific Research (NWO-ALW to A.V.S). The authors thank: Carmel Daunt and Mariam Sofi for technical assistance; Errin Johnson (Sir William Dunn School of Pathology, University of Oxford) for scanning EM, Josh Lorimer, Aaron Moldrich, and Gabriela Panoschi for animal care; David Vremec and Ken Shortman for the gift of antibodies, staff of Monash Micro Imaging for assistance with in vivo DC imaging experiments, Gabrielle Belz for the gift of OT-I Ly5.1 mice, and Drs Michel Nussenzweig and Wolfgang Weninger for the gift of CD11c-YFP mice.

Conflict of interest: The authors declare no financial or commercial conflict of interest.

References

1 **Reis e Sousa, C.**, Dendritic cells in a mature age. *Nat. Rev. Immunol.* 2006. **6**: 476–483.

2 **Hemler, M. E.**, Tetraspanin functions and associated microdomains. *Nat. Rev. Mol. Cell Biol.* 2005. **6**: 801–811.

3 **Rubinstein, E.**, The complexity of tetraspanins. *Biochem. Soc. Trans.* 2011. **39**: 501–505.

4 **Levy, S. and Shoham, T.**, The tetraspanin web modulates immune-signalling complexes. *Nat. Rev. Immunol.* 2005. **5**: 136–148.

5 **Wright, M. D., Moseley, G. W. and van Spriel, A. B.**, Tetraspanin microdomains in immune cell signalling and malignant disease. *Tissue Antigens* 2004. **64**: 533–542.

6 **Figdor, C. G. and van Spriel, A. B.**, Fungal pattern-recognition receptors and tetraspanins: partners on antigen-presenting cells. *Trends Immunol.* 2010. **31**: 91–96.

7 **Flinn, I. W.**, CD37: the comeback kid. *Blood* 2011. **118**: 4007–4008.

8 **Heider, K. H., Kiefer, K., Zenz, T., Volden, M., Stilgenbauer, S., Ostermann, E., Baum, A. et al.**, A novel Fc-engineered monoclonal antibody to CD37 with enhanced ADCC and high proapoptotic activity for treatment of B-cell malignancies. *Blood* 2011. **118**: 4159–4168.

9 **Meyer-Wentrup, F., Figdor, C. G., Ansems, M., Brossart, P., Wright, M. D., Adema, G. J. and van Spriel, A. B.**, Dectin-1 interaction with tetraspanin CD37 inhibits IL-6 production. *J. Immunol.* 2007. **178**: 154–162.

10 **Knobeloch, K. P., Wright, M. D., Ochsenbein, A. F., Liesenfeld, O., Lohler, J., Zinkernagel, R. M., Horak, I. et al.**, Targeted inactivation of the tetraspanin CD37 impairs T-cell-dependent B-cell response under suboptimal costimulatory conditions. *Mol. Cell Biol.* 2000. **20**: 5363–5369.

11 **van Spriel, A. B., de Keijzer, S., van der Schaaf, A., Gartlan, K. H., Sofi, M., Light, A., Linssen, P. C. et al.**, The tetraspanin CD37 orchestrates the alpha4beta1 integrin-Akt signaling axis and supports long-lived plasma cell survival. *Sci. Signal* 2012. **5**: ra82.

12 **van Spriel, A. B., Sofi, M., Gartlan, K. H., van der Schaaf, A., Verschueren, I., Torensma, R., Raymakers, R. A. et al.**, The tetraspanin protein CD37 regulates IgA responses and anti-fungal immunity. *PLoS Pathog.* 2009. **5**: e1000338.

13 **Rops, A. L., Figdor, C. G., van der Schaaf, A., Tamboer, W. P., Bakker, M. A., Berden, J. H., Dijkman, H. B. et al.**, The tetraspanin CD37 protects against glomerular IgA deposition and renal pathology. *Am. J. Pathol.* 2010. **176**: 2188–2197.

14 **van Spriel, A. B., Puls, K. L., Sofi, M., Pouniotis, D., Hochrein, H., Orinska, Z., Knobeloch, K. P. et al.**, A regulatory role for CD37 in T cell proliferation. *J. Immunol.* 2004. **172**: 2953–2961.

15 **Sheng, K. C., van Spriel, A. B., Gartlan, K. H., Sofi, M., Apostolopoulos, V., Ashman, L. and Wright, M. D.**, Tetraspanins CD37 and CD151 differentially regulate Ag presentation and T-cell co-stimulation by DC. *Eur. J. Immunol.* 2009. **39**: 50–55.

16 **Gartlan, K. H., Belz, G. T., Tarrant, J. M., Minigo, G., Katsara, M., Sheng, K. C., Sofi, M. et al.**, A complementary role for the tetraspanins CD37 and Tssc6 in cellular immunity. *J. Immunol.* 2010. **185**: 3158–3166.

17 **Shankaran, V., Ikeda, H., Bruce, A. T., White, J. M., Swanson, P. E., Old, L. J. and Schreiber, R. D.**, IFNgamma and lymphocytes prevent primary tumour development and shape tumour immunogenicity. *Nature* 2001. **410**: 1107–1111.

18 **Lees, C. J., Apostolopoulos, V., Acres, B., Ramshaw, I., Ramsay, A., Ong, C. S. and McKenzie, I. F.**, Immunotherapy with mannan-MUC1 and IL-12 in MUC1 transgenic mice. *Vaccine* 2000. **19**: 158–162.

19 **Derossi, D., Calvet, S., Trembleau, A., Brunissen, A., Chassaing, G. and Prochiantz, A.**, Cell internalization of the third helix of the Antennapedia homeodomain is receptor-independent. *J. Biol. Chem.* 1996. **271**: 18188–18193.

20 **Mosmann, T. R. and Coffman, R. L.**, TH1 and TH2 cells: different patterns of lymphokine secretion lead to different functional properties. *Annu. Rev. Immunol.* 1989. **7**: 145–173.

21 **Barreiro, O., Yanez-Mo, M., Sala-Valdes, M., Gutierrez-Lopez, M. D., Ovalle, S., Higginbottom, A., Monk, P. N. et al.**, Endothelial tetraspanin microdomains regulate leukocyte firm adhesion during extravasation. *Blood* 2005. **105**: 2852–2861.

22 **Zoller, M.**, Tetraspanins: push and pull in suppressing and promoting metastasis. *Nat. Rev. Cancer* 2009. **9**: 40–55.

23 **Czeloth, N., Bernhardt, G., Hofmann, F., Genth, H. and Forster, R.**, Sphingosine-1-phosphate mediates migration of mature dendritic cells. *J. Immunol.* 2005. **175**: 2960–2967.

24 **Henri, S., Vremec, D., Kamath, A., Waithman, J., Williams, S., Benoist, C., Burnham, K. et al.**, The dendritic cell populations of mouse lymph nodes. *J. Immunol.* 2001. **167**: 741–748.

25 **Lindquist, R. L., Shakhar, G., Dudziak, D., Wardemann, H., Eisenreich, T., Dustin, M. L. and Nussenzweig, M. C.**, Visualizing dendritic cell networks in vivo. *Nat. Immunol.* 2004. **5**: 1243–1250.

26 **Ng, L. G., Hsu, A., Mandell, M. A., Roediger, B., Hoeller, C., Mrass, P., Iparraguirre, A. et al.**, Migratory dermal dendritic cells act as rapid sensors of protozoan parasites. *PLoS Pathog.* 2008. **4**: e1000222.

27 **Goschnick, M. W., Lau, L. M., Wee, J. L., Liu, Y. S., Hogarth, P. M., Robb, L. M., Hickey, M. J. et al.**, Impaired "outside-in" integrin alphaIIbbeta3 signaling and thrombus stability in TSSC6-deficient mice. *Blood* 2006. **108**: 1911–1918.

28 **Quast, T., Eppler, F., Semmling, V., Schild, C., Homsi, Y., Levy, S., Lang, T. et al.**, CD81 is essential for the formation of membrane protrusions and regulates Rac1-activation in adhesion-dependent immune cell migration. *Blood* 2011. **118**: 1818–1827.

29 **Lammerding, J., Kazarov, A. R., Huang, H., Lee, R. T. and Hemler, M. E.**, Tetraspanin CD151 regulates alpha6beta1 integrin adhesion strengthening. *Proc. Natl. Acad. Sci. U S A* 2003. **100**: 7616–7621.

30 **Lau, L. M., Wee, J. L., Wright, M. D., Moseley, G. W., Hogarth, P. M., Ashman, L. K. and Jackson, D. E.**, The tetraspanin superfamily member CD151 regulates outside-in integrin alphaIIbbeta3 signaling and platelet function. *Blood* 2004. **104**: 2368–2375.

31 **Feigelson, S. W., Grabovsky, V., Shamri, R., Levy, S. and Alon, R.**, The CD81 tetraspanin facilitates instantaneous leukocyte VLA-4 adhesion strengthening to vascular cell adhesion molecule 1 (VCAM-1) under shear flow. *J. Biol. Chem.* 2003. **278**: 51203–51212.

32 **Ma, J., Wang, J. H., Guo, Y. J., Sy, M. S. and Bigby, M.**, In vivo treatment with anti-ICAM-1 and anti-LFA-1 antibodies inhibits contact sensitization-induced migration of epidermal Langerhans cells to regional lymph nodes. *Cell Immunol.* 1994. **158**: 389–399.

33 **Price, A. A., Cumberbatch, M., Kimber, I. and Ager, A.**, Alpha 6 integrins are required for Langerhans cell migration from the epidermis. *J. Exp. Med.* 1997. **186**: 1725–1735.

34 **Xu, H., Guan, H., Zu, G., Bullard, D., Hanson, J., Slater, M. and Elmets, C. A.**, The role of ICAM-1 molecule in the migration of Langerhans cells in the skin and regional lymph node. *Eur. J. Immunol.* 2001. **31**: 3085–3093.

35 **Lammermann, T., Bader, B. L., Monkley, S. J., Worbs, T., Wedlich-Soldner, R., Hirsch, K., Keller, M. et al.**, Rapid leukocyte migration by integrin-independent flowing and squeezing. *Nature* 2008. **453**: 51–55.

36 **Renkawitz, J., Schumann, K., Weber, M., Lammermann, T., Pflicke, H., Piel, M., Polleux, J. et al.**, Adaptive force transmission in amoeboid cell migration. *Nat. Cell Biol.* 2009. **11**: 1438–1443.

37 **Sala-Valdes, M., Ursa, A., Charrin, S., Rubinstein, E., Hemler, M. E., Sanchez-Madrid, F. and Yanez-Mo, M.**, EWI-2 and EWI-F link the tetraspanin web to the actin cytoskeleton through their direct association with ezrin-radixin-moesin proteins. *J. Biol. Chem.* 2006. **281**: 19665–19675.

38 **Crotta, S., Ronconi, V., Ulivieri, C., Baldari, C. T., Valiante, N. M., Abrignani, S. and Wack, A.**, Cytoskeleton rearrangement induced by tetraspanin engagement modulates the activation of T and NK cells. *Eur. J. Immunol.* 2006. **36**: 919–929.

39 **Pouniotis, D. S., Esparon, S., Apostolopoulos, V. and Pietersz, G. A.**, Whole protein and defined CD8(+) and CD4(+) peptides linked to penetratin targets both MHC class I and II antigen presentation pathways. *Immunol. Cell Biol.* 2011. **89**: 904–913.

40 **Hickey, M. J., Bullard, D. C., Issekutz, A. and James, W. G.**, Leukocyte-endothelial cell interactions are enhanced in dermal postcapillary venules of MRL/fas(lpr) (lupus-prone) mice: roles of P- and E-selectin. *J. Immunol.* 2002. **168**: 4728–4736.

41 **Norman, M. U., Hulliger, S., Colarusso, P. and Kubes, P.**, Multichannel fluorescence spinning disk microscopy reveals early endogenous CD4 T cell recruitment in contact sensitivity via complement. *J. Immunol.* 2008. **180**: 510–521.

Abbreviations: **BMDC**: bone marrow-derived dendritic cell · **DLN**: draining lymph nodes · **MHC-II**: MHC Class II · **Muc1**: Mucin 1 · **SEM**: scanning electron microscopy · **YFP**: yellow fluorescent protein

Full correspondence: Dr. Mark D. Wright, Department of Immunology, Monash University, Alfred Medical Research and Education Precinct (AMREP), Commercial Road, Melbourne, Victoria 3004, Australia
Fax: +61-3 9903 0038
e-mail: Mark.Wright@monash.edu

Received: 8/6/2012
Revised: 3/1/2013
Accepted: 13/2/2013
Accepted article online: 19/2/2013

